Hyperpolarized xenon NMR and MRI signal amplification by gas extraction

Xin Zhou, Dominic Graziani, and Alexander Pines[1]

Materials Sciences Division, Lawrence Berkeley National Laboratory and Department of Chemistry, University of California, Berkeley, CA 94720

Contributed by Alexander Pines, August 13, 2009 (sent for review July 29, 2009)

A method is reported for enhancing the sensitivity of NMR of dissolved xenon by detecting the signal after extraction to the gas phase. We demonstrate hyperpolarized xenon signal amplification by gas extraction (Hyper-SAGE) in both NMR spectra and magnetic resonance images with time-of-flight information. Hyper-SAGE takes advantage of a change in physical phase to increase the density of polarized gas in the detection coil. At equilibrium, the concentration of gas-phase xenon is ≈10 times higher than that of the dissolved-phase gas. After extraction the xenon density can be further increased by several orders of magnitude by compression and/or liquefaction. Additionally, being a remote detection technique, the Hyper-SAGE effect is further enhanced in situations where the sample of interest would occupy only a small proportion of the traditional NMR receiver. Coupled with targeted xenon biosensors, Hyper-SAGE offers another path to highly sensitive molecular imaging of specific cell markers by detection of exhaled xenon gas.

remote detection | dissolved-phase xenon MRI | molecular imaging | phase transition

Magnetic resonance imaging (MRI) is a powerful technology, capable of routine and noninvasive imaging of the internal structures and functions of a multitude of subjects ranging from biological samples in medical imaging to porous media in materials science (1–4). Conventional MRI focuses mainly on the nuclear spin of the proton because it is ubiquitous in most parts of the human body. However, certain organs like the lungs have a low proton spin density attributable to the large volume of air dispersed throughout the tissue. The low sensitivity of traditional magnetic resonance has motivated the development of techniques using hyperpolarized noble gases for NMR and MRI (5, 6). Hyperpolarized noble gases can provide signal enhancements of 10,000 to 100,000 times that of thermally polarized gases (7, 8), making it possible to obtain magnetic resonance images of the lung airspace with unprecedented spatial resolution and sensitivity (9, 10). Xenon also has the unique characteristic of being soluble in many fluids and biological tissues, such as water, blood, lung tissue, and white and gray matter (11–13). Being a trace element in the atmosphere, xenon has no natural background signal in the human body (11–13). Therefore, dissolved-phase xenon MRI and molecular imaging could provide rich information related to biological and physiological changes beyond void space lung imaging. Efforts have demonstrated the value of dissolved xenon MRI in the study of lung gas exchange (14–16), and brain perfusion (17–20).

Xenon-based molecular imaging has been demonstrated by using cryptophane-containing biosensors (21). Sensitivity enhancement using a chemical amplification technique, hyperpolarized xenon chemical exchange saturation transfer (Hyper-CEST) (22), allows imaging at low concentrations; however, for in vivo applications the small filling factor of a region of interest in the body relative to the NMR coil is a significant factor limiting sensitivity. In such cases remote detection methods (23, 24) can provide dramatic improvements in sensitivity. In remote detection, the normal NMR coil that contains the full region of interest is used to encode spectroscopic and spatial information, then stores it as longitudinal magnetization. These encoded spins then flow into a second coil with an optimized filling factor for detection.

Remote detection can overcome the filling factor issue of dissolved xenon MRI, although a low concentration of xenon in solution can be another significant impediment to highly sensitive detection (25). It has been shown that the solvated xenon signal can be amplified by xenon polarization transfer contrast (15), in which the dissolved-phase xenon is selectively saturated, and through exchange, the gas-phase signal is attenuated. This method is able to indirectly image dissolved-phase xenon, but is limited to tissue in direct exchange with the air in the lungs. The gas exchange process could be similarly exploited for direct signal amplification of dissolved xenon with the remote detection technique. Xenon gas can be extracted from the dissolved solutions and concentrated in the gas phase for detection. Furthermore, with the long longitudinal relaxation time of gas-phase xenon (11–13), extracted xenon gas from solution can be compressed or liquefied while preserving the encoded information. The xenon density in the liquid state is approximately four orders of magnitude higher than in aqueous solutions (11–13), which in principle could result in up to 10,000 times enhancement of spin density, thus allowing substantial signal amplification.

In this article, we demonstrate the hyperpolarized xenon signal amplification by gas extraction (Hyper-SAGE) method with enhanced NMR spectra and time-of-flight (TOF) images by using recently commercialized membrane technology for high-efficiency xenon dissolution (26). The Hyper-SAGE technique relies on physical amplification by exploiting a phase change and is completely distinct from chemical amplification. In combination with additional amplification techniques such as Hyper-CEST, this method promises to dramatically decrease the detection threshold of MRI and has the potential to benefit molecular imaging applications and medical diagnostics. Moreover, because the polarization of hyperpolarized xenon does not depend on the magnetic field strength, this technique could also be applied for use with low field portable MRI devices (27–29).

Results and Discussion

A remotely detected spectrum of xenon dissolved in water and a set of remotely detected time-of-flight (TOF) images were obtained for the first demonstrations of Hyper-SAGE. Fig. 1*A* shows an NMR spectrum of xenon dissolved in water by using the direct detection scheme of pulse and acquire. Fig. 1*B* is the same spectrum acquired by using the Hyper-SAGE method, where the spectral information is encoded in the dissolved phase and detected at a later time in the gas phase (see Fig. 3). Not only has the spectrum been replicated accurately, but comparison of the remote and direct spectra shows an enhancement in the signal-

Author contributions: X.Z., D.G., and A.P. designed research; X.Z. and D.G. performed research; X.Z. and D.G. analyzed data; and X.Z., D.G., and A.P. wrote the paper.

The authors declare no conflict of interest.

Freely available online through the PNAS open access option.

[1]To whom correspondence should be addressed. E-mail: pines@berkeley.edu.

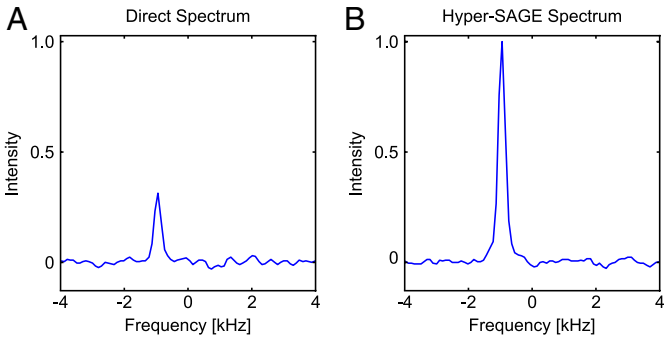

Fig. 1. Directly detected spectrum (*A*) and remotely detected Hyper-SAGE spectrum (*B*) of ^{129}Xe dissolved in water. Both spectra were scaled by their respective noise levels, and an intensity of 1.0 was assigned to maximum signal in the remote spectrum. The same sample was used in both experiments with the detection coil of the direct spectrum being used as the encoding coil for the remote spectrum. Xenon gas is extracted from the encoding volume and flows to the detection coil in the remote experiment, resulting in an increased concentration of hyperpolarized Xe and hence an increase in SNR of ≈3. Despite being detected at a later time, in a different location, and a different physical state, the original xenon in water spectrum is reproduced exactly.

to-noise ratio (SNR) of ≈3. This enhancement comes about because of the higher concentration of xenon as a gas relative to xenon dissolved in water. With the current implementation in which the extracted gas is neither compressed nor cooled, the maximum theoretical signal enhancement caused by the change in concentration is ≈9, determined by the Ostwald solubility coefficient at room temperature (30). For this experiment, the xenon gas mixture was dissolved in water with a pressure of 50 psi (340 kPa); however, to decrease the travel time from the extraction membrane to the detector, the gas was extracted under vacuum with a pressure of 4 psi (28 kPa). Under these conditions, the maximum enhancement caused by the concentration difference is ≈4.4. To ensure the observed signal enhancement was caused by the concentration difference and not a more traditional remote detection enhancement, the filling factor of both the encoding coil and the detection coil were made to be equal. The quality factor (Q) of the detection coil is 1.4 times higher than that of the encoding coil, leading to an additional sensitivity of 18%, which is small compared with the overall achieved enhancement.

Images of xenon dissolved in water in the cylindrical encoding phantom were also acquired as a function of the TOF from the encoding coil to the detection coil (Fig. 2). Once the encoded spins reach the detector, the acquisition is repeated in intervals of the sample's residence time in the coil until all of the encoded spins have traveled through the detection coil. The first spins reaching the detector come from the outlet of the encoding phantom. The total travel time for these nuclei to travel from the encoding coil, through the gas extraction membrane, and into the detection coil is 11 s. From a TOF of 17–41 s, encoded spins from the main body of the encoding phantom reach the detector, and finally after 47 s, the encoded xenon nuclei from the inlet of the phantom are detected.

These results demonstrate that the dissolved-phase NMR spectrum of xenon can be obtained via remotely detecting the extracted xenon in the gas phase. Spatial information can also be encoded to obtain TOF images. The encoded phase of hyperpolarized xenon spins is stored as the longitudinal magnetization and therefore survives the travel through magnetic field gradients and, more importantly, a phase change. Additionally, xenon gas has a very long longitudinal relaxation time so encoded information can persist for an extended period as can be seen in the TOF images (Fig. 2). This persistence of magnetization allows ample time to prepare the xenon for optimal detection SNR. Through gas compression or liquefaction, the density of xenon could be increased on the order of 10^4 times over xenon dissolved in water. Because remote detection is a point-by-point method, the time needed to acquire remote data scales with the number of points and therefore can take considerably longer than direct detection. However, in situations with samples of low concentration and low filling factor, the signal amplification attainable by Hyper-SAGE surpasses direct signal averaging over a comparable time period.

With the potential of a very large signal enhancement combined with TOF imaging (unattainable by conventional MRI), Hyper-SAGE seems to be a promising method for studying gas exchange. The TOF images shown in Fig. 2 contain information about the geometry of the encoding environment and the flow path of the water. By including membrane material in the encoding phantom, properties of the gas exchange across the membrane could also be determined by both the TOF properties

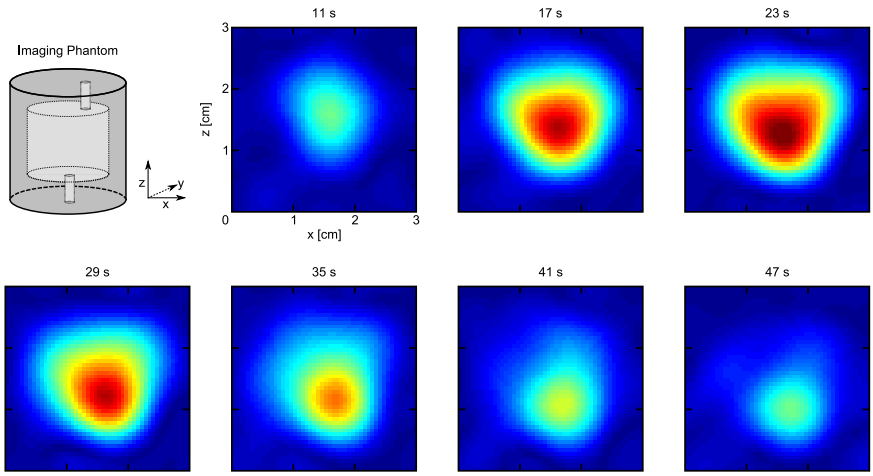

Fig. 2. TOF Hyper-SAGE images of xenon dissolved in water continuously flowing through the encoding phantom depicted in the *Upper Left*. Each image is labeled with its average TOF. The flow is along the positive *z*-direction, and as such, signal from the top of the phantom at the outlet reaches the detection coil first. Over time, successive portions of the encoded volume are detected until the remaining signal is recovered after 47 s of travel time. The absence of signal at the bottom edges of the encoding phantom is likely caused by flow vortices at the inlet preventing the xenon spins from reaching the detector within the longitudinal relaxation time.

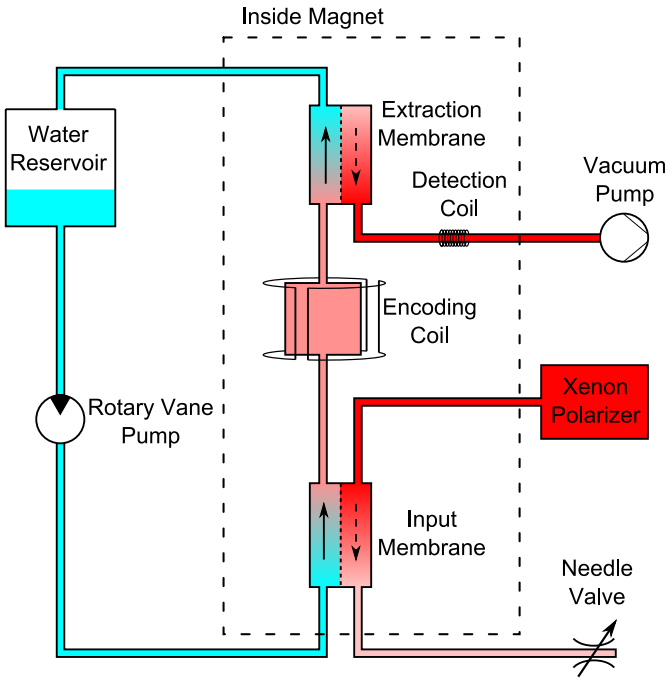

Fig. 3. Schematic of the experimental setup. Blue and red shading represent the water and gas flow paths, respectively. The intensity of the red coloring indicates the concentration of hyperpolarized xenon. Distilled water initially flows to the input membrane contactor where it comes into contact with hyperpolarized xenon produced by a homebuilt polarizer. The aqueous xenon solution then flows to an encoding coil where either spectral or spatial information is encoded into the sample. Finally, the solution travels to the extraction membrane contactor where the encoded hyperpolarized xenon is extracted into the gas phase and detected in the detection coil.

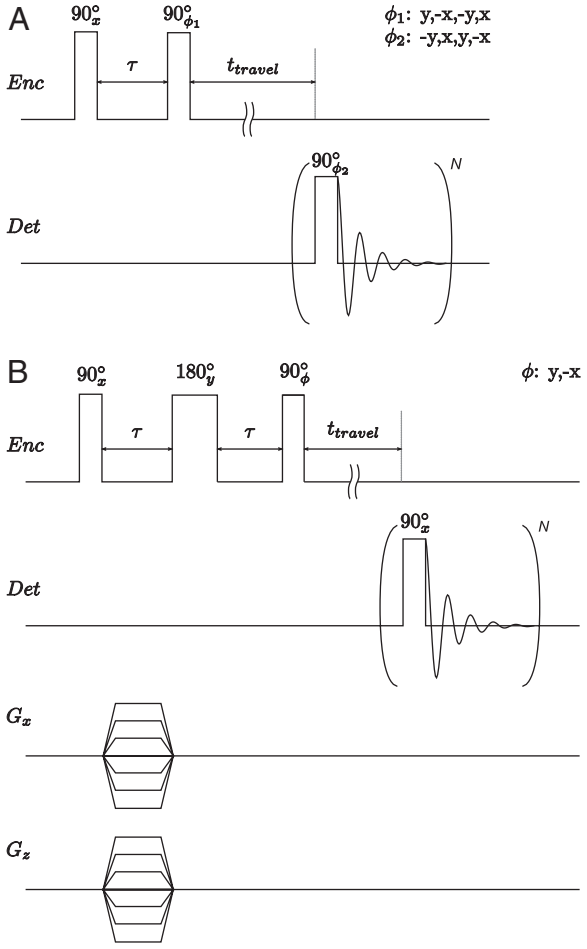

Fig. 4. Remote detection pulse sequences. (*A*) Remote spectroscopy. Initially, a 90° pulse is applied to excite the sample into the transverse plane. The spins are allowed to evolve under chemical shift for a time τ, at which point a second 90° pulse is applied to store the encoded information along the longitudinal axis. The spins then travel to the detection coil where the information is read out with a train of excitation pulses. (*B*) The pulse sequence for the remote images is similar to the remote spectroscopy; however, instead of evolving under chemical shift, spatial information is encoded with phase-encode gradients in the *x* and *z* directions. A 180° pulse is also applied before storage to refocus any static field inhomogeneities.

of the encoded spins and encoded diffusion information through the gradient (31). The intrinsically low filling factors in membrane environments provide additional motivation for a remote detection experiment such as Hyper-SAGE. By adopting a microcoil for detection, as is used in microfluidic remote detection (24, 32), extremely high time resolution of the gas exchange process can be achieved to study membrane materials such as the gas exchange membranes used in this experiment or biological samples such as lung tissues.

In conclusion, we have demonstrated a method to amplify the solvated hyperpolarized NMR and MRI signals via remote detection of the extracted gas. This method provides a signal enhancement caused by concentration differences between dissolved xenon and gas-phase xenon and can be combined with remote detection enhancements in any environment with a low filling factor. Further amplification can be accomplished by either compressing or liquefying the extracted gas. Finally, Hyper-SAGE is also compatible with chemical exchange amplification techniques such as Hyper-CEST, making it a valuable tool for diagnostics and molecular imaging in addition to gas exchange studies.

Materials and Methods

Hyperpolarized Xenon. A homebuilt xenon polarizer produces hyperpolarized ^{129}Xe by spin-exchange optical pumping (7). The apparatus is similar to that in ref. 33 except that the current setup allows for continuous gas flow. A gas mixture of 2% natural abundance Xe, 2% N_2, and 96% He flows through an optical pumping cell filled with Rb vapor at 140 C°. Three laser diode arrays optically pump the Rb at 794.7 nm with 110 W of total laser power. Typical polarization levels of 8–10% are achieved at a flow rate of 0.5 standard liters per minute (SLPM).

Flow Setup. Hyperpolarized ^{129}Xe is dissolved and extracted in three independent flow paths as depicted in Fig. 3. Xenon flows from the polarizer at 0.5 SLPM and a pressure of 50 psi (340 kPa), where it encounters the first of two membrane modules (Membrana model G543; 16-mL liquid volume, 25-mL gas volume). This module allows the gas to come into contact with recirculating distilled water pressurized to 80 psi (550 kPa) and flowing at a rate of 2 mL/s. The large surface area of the membrane module enables rapid dissolution of hyperpolarized xenon into the water. The water then flows into a cylindrical phantom (10.8 mL) inside a 38-mm saddle-shaped encoding coil where the NMR information is encoded into the longitudinal magnetization at 9.4 T. The solvated xenon continues flowing to a second membrane module (Membrana model G591; ≈1-mL liquid volume, 2.7-mL gas volume) where it is extracted from the liquid under a vacuum of 4 psi (28 kPa). The extracted gas is then detected with a 3.2-mm i.d., 1-cm long solenoid detection coil with a detection volume of 0.02 mL.

Pulse Sequences. The pulse sequences for the remotely detected spectrum and the remotely detected TOF images are depicted in Fig. 4 *A* and *B*, respectively. Both sequences follow the basic remote detection format where the magnetization in the encoding volume is excited, allowed to evolve, then stored to the longitudinal axis. The encoded spins then flow to the detection coil where the *z*-magnetization is read out with a series of excitation pulses. Because each storage pulse only stores one component of the magnetization, a minimum of

two phase cycles is needed to collect both the real and imaginary components of the data. For the remotely detected spectrum, the spins are allowed to evolve under chemical shift for a time τ, which is then incremented to reconstruct the free induction decay (FID) point by point. To acquire the TOF images, the spins evolve under two phase encode gradients applied in the *z* and *x* directions to encode the spatial information. A 180° pulse is then applied at a time τ to refocus the effects of any static field inhomogeneities. Finally, at time 2τ, the encoded information is stored along the *z* axis and the spins flow to the detection coil to be decoded. A four-step phase cycle involving both the storage and detection pulses was used to acquire the remote spectrum to remove the baseline offset of the FID produced by unencoded spins in the detection coil. The TOF images were collected with only a two-step phase cycle of the storage pulse to save on acquisition time.

Data Reconstruction. ***Spectrum.*** Because of the four-step phase cycle used in acquiring the remote spectrum, only encoded spins contribute to the signal in the detection coil. Optimal signal-to-noise can be obtained by acquiring the entire encoded volume in one acquisition; however, because of the large volume of extracted gas compared with the detection volume, the encoded spins were detected over 60 acquisitions. Each FID collected from the individual detection pulses was first apodized with a matched exponential function, and then Fourier-transformed. All points in the TOF dimension were added together to reproduce as much of the original signal from the encoding phantom as possible. This process was repeated over the bandwidth of the detected gas signal, and each reconstructed FID was added to produce the final remotely detected FID. Both the remotely detected and directly detected signals were first zero-filled from the original 41 points to a total of 82 points and apodized with the same Hamming function to reduce truncation artifacts before Fourier transformation.

Images. The TOF images were processed in a similar manner as the remote spectrum, with baseline correction applied to remove a dc offset caused by the reduced two-step phase cycle. Additionally, the TOF dimension was exploited to reconstruct images as a function of the time taken to reach the detector. Each TOF image was averaged over 12 TOF points. All images were acquired with a resolution of $\approx$6 mm and seven phase encode steps in each dimension. Data were apodized with a Gaussian function and zero-filled to 64×64 points before Fourier transforming.

ACKNOWLEDGMENTS. We thank Prof. David Wemmer and Dr. Vikram Bajaj for critical reading and helpful suggestions on the manuscript. This work was supported by the Director, Office of Science, Office of Basic Energy Sciences, Materials Sciences Division, of the U.S. Department of Energy under Contract DE-AC02-05CH11231.

1. Lauterbur PC (1973) Imaging formation by induced local interactions: Examples employing nuclear magnetic resonance. *Nature* 242:190–191.
2. Kumar A, Welti D, Ernst RR (1975) NMR Fourier zeugmatography. *J Magn Reson* 18:69–83.
3. Blümich B (2000) *NMR Imaging of Materials* (Oxford Univ Press, Oxford).
4. Callaghan PT (1991) *Principles of Nuclear Magnetic Resonance Microscopy* (Clarendon, New York).
5. Raftery D, et al. (1991) High field NMR of adsorbed xenon polarized by laser pumping. *Phys Rev Lett* 66:584–587.
6. Albert MS, et al. (1994) Biological magnetic resonance imaging using laser-polarized ^{129}Xe. *Nature* 370:199–201.
7. Walker TG, Happer W (1997) Spin-exchange optical pumping of noble-gas nuclei. *Rev Mod Phys* 69:629–642.
8. Zhou X, et al. (2004) Production of hyperpolarized ^{129}Xe gas without nitrogen by optical pumping at ^{133}Cs D_2 line in flow system. *Chin Phys Lett* 21:1501–1503.
9. Saam BT, et al. (2000) MR imaging of diffusion of ^{3}He gas in healthy and diseased lungs. *Magn Reson Med* 44:174–179.
10. Möller HE, et al. (2002) MRI of the lungs using hyperpolarized noble gases. *Magn Reson Med* 47:1029–1051.
11. Cherubini A, Bifone A (2003) Hyperpolarized xenon in biology. *Prog Nucl Magn Reson Spectr* 42:1–30.
12. Oros A-M, Shah NJ (2004) Hyperpolarized xenon in NMR and MRI. *Phys Med Biol* 49:R105–R153.
13. Goodson BM (2002) Nuclear magnetic resonance of laser-polarized noble gases in molecules, materials, and organisms. *J Magn Reson* 155:157–216.
14. Swanson SD, Rosen MS, Coulter KP, Welsh RC, Chupp TE (1999) Distribution and dynamics of laser-polarized ^{129}Xe magnetization in vivo. *Magn Reson Med* 42:1137–1145.
15. Ruppert K, Brookeman JR, Hagspiel KD, Mugler JP, III (2000) Probing lung physiology with xenon polarization transfer contrast (XTC). *Magn Reson Med* 44:349–357.
16. Driehuys B, et al. (2006) Imaging alveolarcapillary gas transfer using hyperpolarized ^{129}Xe MRI. *Proc Natl Acad Sci USA* 103:18278–18283.
17. Swanson SD, et al. (1997) Brain MRI with laser-polarized ^{129}Xe. *Magn Reson Med* 38:695–698.
18. Duhamel G, et al. (2002) Global and regional cerebral blood flow measurements using NMR of injected hyperpolarized xenon 129. *Acad Radiol Suppl* 2:S498–S500.
19. Kilian W, Seifert F, Rinneberg H (2004) Dynamic NMR spectroscopy of hyperpolarized ^{129}Xe in human brain analyzed by an uptake model. *Magn Reson Med* 51:843–847.
20. Zhou X, et al. (2008) Reinvestigating hyperpolarized ^{129}Xe longitudinal relaxation time in the rat brain with noise considerations. *NMR Biomed* 21:217–225.
21. Hilty C, Lowery TJ, Wemmer DE, Pines A (2006) Spectrally resolved magnetic resonance imaging of a xenon biosensor. *Angew Chem Int Ed* 45:70–73.
22. Schröder L, Lowery TJ, Hilty C, Wemmer DE, Pines A (2006) Molecular imaging using a targeted magnetic resonance hyperpolarized biosensor. *Science* 314:446–449.
23. Moulé AJ, et al. (2003) Amplification of xenon NMR and MRI by remote detection. *Proc Natl Acad Sci USA* 100:9122–9127.
24. Hilty C, et al. (2005) Microfluidic gas-flow profiling using remote-detection NMR. *Proc Natl Acad Sci USA* 102:14960–14963.
25. Moulé AJ (2003) Ex situ and remote detection nuclear magnetic resonance. PhD dissertation (Univ of California, Berkeley).
26. Baumer D, Brunner E, Blümler P, Zänker PP, Spiess HW (2006) NMR spectroscopy of laser-polarized ^{129}Xe under continuous flow: A method to study aqueous solutions of biomolecules. *Angew Chem Int Ed* 45:7282–7284.
27. Appelt S, Häsing FW, Kühn H, Perlo J, Blümich B (2005) Mobile high-resolution xenon nuclear magnetic resonance spectroscopy in the Earth's magnetic field. *Phys Rev Lett* 94:197602.
28. Blümich B, Perlo J, Casanova F (2008) Mobile single-sided NMR. *Prog Nucl Magn Reson Spectr* 52:197–269.
29. Paulsen JL, Bouchard L-S, Graziani D, Blümich B, Pines A (2008) Volume-selective magnetic resonance imaging using an adjustable, single-sided, portable sensor. *Proc Natl Acad Sci* 105:20601–20604.
30. Clever HL, Battino R (1979) *Krypton, Xenon, and Radon: Gas Solubilities* (Pergamon, Oxford), Vol 2.
31. Telkki V-V, Hilty C, Garcia S, Harel E, Pines A (2007) Quantifying the diffusion of a fluid through membranes by double phase encoded remote detection magnetic resonance imaging. *J Phys Chem B* 111:13929–13936.
32. Harel E, Pines A (2008) Spectrally resolved flow imaging of fluids inside a microfludic chip with ultrahigh time resolution. *J Magn Reson* 193:199–206.
33. Zhou X, et al. (2004) Experimental and dynamic simulations of radiation damping of laser-polarized liquid ^{129}Xe at low magnetic field in a flow system. *Appl Magn Reson* 26:327–337.